Correcting for a density distribution: particle size analysis of core-shell nanocomposite particles using disk centrifuge photosedimentometry

Lee A. Fielding, Oleksandr O. Mykhaylyk, Steven P. Armes, Patrick W. Fowler**

Dainton Building, Department of Chemistry, The University of Sheffield,

Brook Hill, Sheffield, South Yorkshire, S3 7HF, UK.

Vikas Mittal[$]

BASF SE, Polymer Physics, 67056 Ludwigshafen, Germany

Stephen Fitzpatrick

CPS Instruments Inc., 7349 SE Seagate Lane, Stuart, Florida, 34997, USA

Abstract. Many types of colloidal particles possess a core-shell morphology. In this paper we show that, if the core and shell densities differ, this morphology leads to an *inherent* density distribution for particles of finite polydispersity. If the shell is denser than the core, this density distribution implies an artificial narrowing of the particle size distribution as determined by disk centrifuge photosedimentometry (DCP). In the specific case of polystyrene/silica nanocomposite particles, which consist of a polystyrene core coated with a monolayer shell of silica nanoparticles, we demonstrate that the particle density distribution can be determined by analytical ultracentrifugation and introduce a mathematical method to account for this density distribution by reanalyzing the raw DCP data. Using the mean silica packing density calculated from small-angle x-ray scattering, the real particle density can be calculated for each data point. The corrected DCP particle size distribution is both broader and more consistent with particle size distributions reported for the same polystyrene/silica nanocomposite sample using other sizing techniques, such as electron microscopy, laser light diffraction and dynamic light scattering. Artifactual narrowing of the size distribution is also likely to occur for many other polymer/inorganic nanocomposite particles comprising a low-density core of variable dimensions coated with a high-density shell of constant thickness, or for core-shell latexes where the shell is continuous rather than particulate in nature.

* Authors to whom correspondence should be addressed (s.p.armes@shef.ac.uk or p.w.fowler@shef.ac.uk).

[$] Present address: Chemical Engineering Department, The Petroleum Institute, Abu Dhabi, United Arab Emirates.

Introduction

Disk centrifuge photosedimentometry (DCP) is a high resolution particle sizing technique that has been widely used in colloid science. [1-35] It reports the weight-average particle diameter, which lies between the number-average and intensity-average diameters obtained from electron microscopy and dynamic light scattering, respectively. DCP has been used to size a wide range of lyophobic colloids, including silica,[1,2] titania,[3,4] barium titanate,[5] carbon nanotubes,[6] pigments,[7] *E. coli*,[8,9] adenovirus,[10] a range of copolymer latexes,[11-16] gold sols[17,18] and various types of nanocomposite particles.[19-31] In addition, DCP can be used to assess the colloidal stability of aqueous dispersions. For example, incipient flocculation induced by adjusting the solution pH,[21,24] the physical adsorption of silica nanoparticles[31] or the deposition of an ultrathin overlayer of a conducting polymer[32-34] is readily detected. Recently, Dawson and co-workers utilized DCP to estimate the thickness of a globular protein adsorbed onto latex particles,[35] whereas Bon et al. monitored the depletion of an ultrafine silica sol from the reaction solution during the formation of polymer/silica colloidal nanocomposite particles.[2] In related work, DCP has been utilized for studying the mechanism of formation of core-shell poly(methyl methacrylate)/silica nanocomposite particles prepared by aqueous emulsion polymerization.[30]

Over the last two decades or so, we have developed various formulations for the synthesis of organic/inorganic hybrid particles, in which the organic phase is either a conducting polymer [19-23] or a vinyl polymer[24-30,36] and the inorganic phase comprises silica nanoparticles. Potential applications for such colloidal nanocomposites include pH-responsive Pickering emulsifiers,[37] synthetic mimics for micrometeorites[38,39] and high performance exterior architectural coatings.[40] Various particle morphologies have been observed, including currant bun,[24,41,42] raspberry,[20,22] and core-shell.[27,30,36] The latter morphology is characteristic of vinyl (co)polymer/silica nanocomposites, which also correspond to the most efficient formulations (i.e. the highest monomer conversions and silica aggregation efficiencies). Here the (co)polymer component forms a low density latex core, while the silica nanoparticles adsorb as a well-defined monolayer to form a high density shell with a relatively constant silica packing density.[43] To a good approximation, the finite width of the size distribution of such nanocomposite particles is due to the polydispersity of the latex cores, rather than variation in the mean shell thickness.

It is well known that SAXS is a powerful characterization technique for the analysis of core-shell colloidal nanocomposite particles.[43-45] The relatively narrow particle size distributions and high electron-density contrast between the polymer core and silica shell allows detailed structural and compositional information to be determined. Balmer *et al.* used time-resolved SAXS to study nanocomposite particles prepared by heteroflocculation of poly(2-vinylpyridine) latex on addition of an ultrafine silica sol.[44,45] In particular, the kinetics of heteroflocculation and also with the redistribution of silica between nanocomposite particles was shown to occur on the millisecond time scale. Of particular relevance to the present study, it was demonstrated that poly(styrene-co-*n*-butyl acrylate)/silica nanocomposite particles prepared by *in situ* copolymerization have a much more ordered particulate silica shell than those prepared by heteroflocculation.[43] This was evident since the former nanocomposites exhibited a prominent shoulder at q values of approximately 0.03 $Å^{-1}$, whereas this structural order feature was absent for the latter nanocomposites. A Percus-Yevick hard-sphere structure factor was introduced to account for the inter-particle interactions between

the close-packed silica particles within the shell and hence produce a good fit to the SAXS data obtained for core-shell nanocomposite particles prepared by in situ copolymerization.[43]

In previous studies, we have routinely used DCP to characterize such nanocomposite particles.[27,30] However, we have only recently realized that their core-shell morphology inevitably leads to a density distribution being superimposed on their particle size distribution. Within a given size population, smaller nanocomposite particles necessarily contain a higher proportion of silica than larger nanocomposite particles (see Figure 1). Since the silica has a significantly higher density than the polystyrene cores (2.16 g cm^{-3} vs. 1.05 g cm^{-3}), it follows that the smaller nanocomposite particles must possess a higher density than the larger nanocomposite particles. If this hypothesis is correct, this leads to a serious problem for DCP analysis, since this instrument only allows a single density value as an input parameter. In the present work, we use analytical ultracentrifugation to confirm the existence of a density distribution for the specific case of polystyrene/silica nanocomposite particles. We demonstrate that DCP analysis of such particles using a single mean density leads to an artificial narrowing of their particle size distribution. Furthermore, we show how to use the density distribution to correct the DCP data and hence obtain a meaningful weight-average particle size distribution for such core-shell nanocomposite particles.

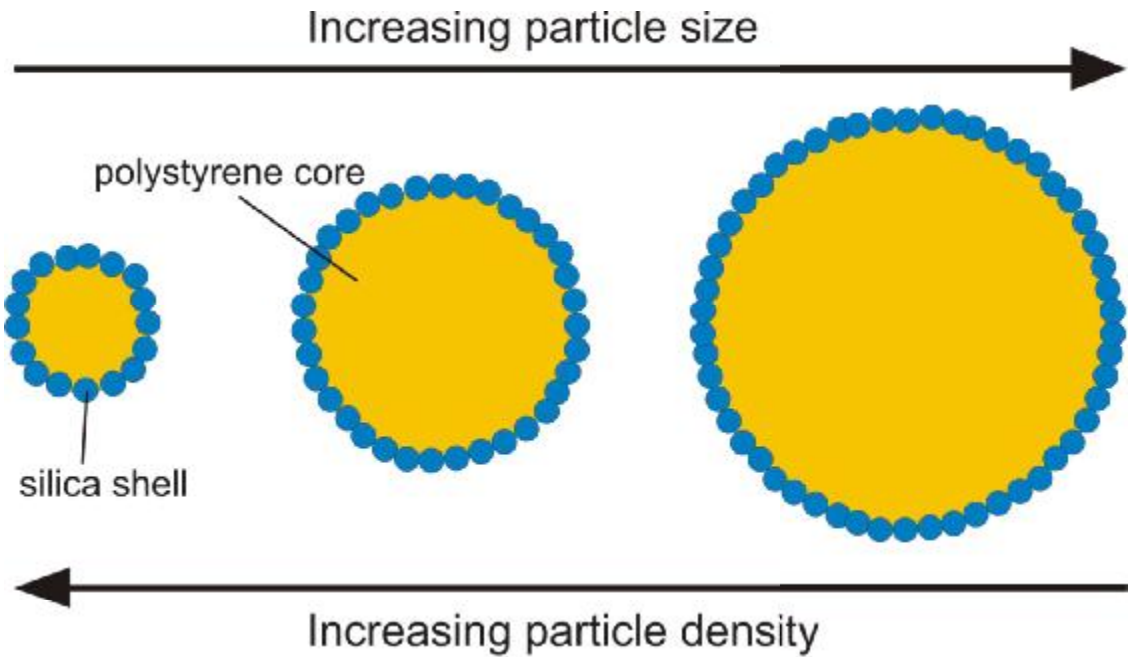

Figure 1. Relationship between particle size and density for polystyrene/silica core-shell nanocomposite particles comprising latex cores of finite polydispersity surrounded by a particulate silica monolayer of uniform thickness.

Experimental

Materials. Styrene was purchased from Aldrich, passed through a basic alumina column to remove inhibitor and then stored at -20 °C prior to use. 2,2'-Azobis(isobutyramidine) dihydrochloride (AIBA) was used as received from Aldrich. Glycerol-functionalized silica sol (Bindzil CC40; 37 wt. % aqueous dispersion; 12 nm nominal diameter) was supplied by Eka Chemicals (Bohus, Sweden), which is a division of AkzoNobel (The Netherlands). BET measurements indicated that the silica particles have a specific surface area of 158 m^2 g^{-1}. Given a silica sol density of 2.16 g cm^{-3} (as determined by helium pycnometry), this suggests a surface-average mean diameter of 18 nm, which is consistent with TEM studies. Deionized water (obtained from an Elgastat Option 3A water purifier) was used in all experiments.

Nanocomposite synthesis. A slightly modified version of the previously reported synthesis of polystyrene/silica nanocomposite particles has been used.[29] Aqueous silica sol (2.0 g) was diluted with water in a round-bottomed flask containing a magnetic stirrer bar, styrene (5.0 g) was added and the solution was degassed with bubbling nitrogen. This was heated to 90 °C in an oil bath followed by the addition of AIBA initiator (50 mg) which had been previously dissolved in 4.0 g water; this gave a total mass of water of 45.0 g. The polymerization was allowed to proceed for 24 h. The resulting colloidal dispersion was purified by repeated centrifugation-redispersion cycles (6000 rpm for 30 min. for five cycles) with each successive supernatant being decanted and replaced with water.

Dynamic light scattering (DLS). Studies were conducted at 25 °C using a Malvern Zetasizer Nano ZS instrument equipped with a 4 mW He-Ne solid-state laser operating at 633 nm. Back-scattered light was detected at 173° and the mean particle diameter was calculated over thirty runs of ten seconds duration from the quadratic fitting of the correlation function using the Stokes-Einstein equation. All measurements were performed in triplicate on a highly dilute aqueous dispersion.

Laser diffraction. A Beckman-Coulter LS 230 particle size analyzer equipped with a variable speed module, polarization intensity differential scattering (PIDS) system and operating at 780 nm was used to obtain a volume-average particle size distribution. The PIDS system uses three wavelengths (450, 600 and 900 nm), which are horizontally and vertically polarized. The optical data for polystyrene was used to obtain the volume-average particle size distributions reported in this work. However, if the refractive index of silica was used instead, it made essentially no difference to either the peak position or width of the reported volume-average particle size distribution.

Disk centrifuge photosedimentometry. A CPS Instruments model DC24000 instrument was used to obtain weight-average particle size distributions. The disk centrifuge was operated at 16 000 rpm and the spin fluid contained a density gradient constructed from 12.0 to 4.0 wt. % aqueous sucrose solutions; a small volume of *n*-dodecane (0.50 ml) was used in order to extend the lifetime of the gradient. The disk centrifuge was calibrated with a poly(vinyl chloride) latex with a weight-average particle diameter of 263 nm.

Helium pycnometry. The solid-state density of both the dried polystyrene/silica nanocomposite particles and the silica sol were measured using a Micromeritics AccuPyc 1330 helium pycnometer at 20 °C.

Thermogravimetric analysis (TGA). Analyses were conducted on freeze-dried particles which were heated in air to 800 °C at a heating rate of 20 °C min^{-1} using a TA Instruments Q500. The observed mass loss was attributed to complete pyrolysis of the copolymer component, with the remaining incombustible residues being attributed to pure silica (SiO_2).

Transmission electron microscopy (TEM). Images were recorded using a Phillips CM100 microscope operating at 100 kV by drying a drop of dilute aqueous nanocomposite dispersion onto a carbon-coated copper grid.

Surface area analysis. BET surface area measurements were performed using a Quantachrome Nova 1000e instrument with dinitrogen as an adsorbate at 77 K. Freeze-dried samples were degassed under vacuum at 60 °C for at least 15 h prior to analysis. The particle diameter, d, was calculated from the formula $d = 6/(\rho A_s)$, where A_s is the BET specific surface area and ρ is the silica sol density obtained from helium pycnometry.

Static density gradients. A modified OPTIMA XL analytical ultracentrifuge (AUC, Beckman Coulter) was used for the static density gradient analysis.[46,47] This instrument is equipped with an eight-hole rotor and custom-built Schlieren optics with a multiplexer. The Schlieren optics set-up was similar to that in a Rayleigh interferometer, but with the addition of a phase plate placed at the focal point of the condenser lens. The radial scans were collected at fixed time intervals in order to ascertain when equilibrium had been attained. Titanium centerpieces were used for the measurements. Mono-sector cells containing -2° horizontal wedge windows were used to compensate for the steep radial optical refractive index gradient. A water (density = 0.9987 g cm^{-3}) – Nycodenz® (density = 2.060 g cm^{-3}) density gradient was used that gave an operating density range of 1.07-1.24 g cm^{-3}. Higher and lower density gradients were also evaluated but these proved to be unnecessary for characterization of this particular polystyrene/silica nanocomposite dispersion. A small amount of emulsifier was also added to water in order to prevent any particle aggregation. The rotor speed was 30 000 rpm and the cells were almost completely filled in order to cover the maximum density range. The polystyrene/silica nanocomposite particles were diluted to a concentration of 0.050 g dm^{-3} and run for 22 h at 25 °C.

Small angle x-ray scattering. Small-angle x-ray scattering (SAXS) patterns were collected at the European Synchrotron Radiation Facility, at Station ID02 (x-ray radiation wavelength, λ = 1 Å, cross-section of the beam at the sample holder = 0.3 mm which was significantly less than the diameter of the quartz capillary sample holder). The x-ray scattering intensity was recorded using a FReLoN (Fast-Readout Low-Noise) Kodak CCD detector over a q range of 0.001-0.07 $Å^{-1}$. Aqueous polystyrene/silica nanocomposite dispersions (1.0 w/v %) were injected into a thin-walled flow-through quartz capillary cell (1.4 mm in diameter with a wall thickness of approximately 10 µm). The SAXS data was reduced (i.e. normalized, regrouped into one-dimensional patterns, desmeared, averaged and background-subtracted) using a utilities software package written by Dr. M. Sztucki.[48]

Results and Discussion

Polystyrene/silica nanocomposite particles. Well-defined polystyrene/silica nanocomposite particles can readily be prepared by aqueous emulsion polymerization of styrene in the presence of a glycerol-modified 18 nm silica sol using a cationic azo initiator at 60 °C (Figure 2).[28,29] This formulation typically leads to relatively monodisperse particles of approximately 200-400 nm diameter with silica contents ranging from 22 to 28 % by mass.[29] Moreover, high silica aggregation efficiencies (up to 95 %) are readily achieved, making this formulation very attractive for the preparation of colloidal nanocomposite particles. It has been previously demonstrated that these nanocomposite particles comprise polystyrene cores and a particulate silica shell by techniques such as electron spectroscopy imaging transmission electron microscopy[29] and SAXS.[43]

The polystyrene/silica particles studied in the current work were prepared using a slightly modified formulation to that described previously.[29] The main difference is that the synthesis was conducted at 90 °C in this work, whereas Schmid *et al.*[29] used a polymerization temperature of 60 °C. This higher temperature results in a somewhat higher polydispersity, as indicated by the representative TEM image of the polystyrene/silica nanocomposite particles shown in Figure 2. It is clear that the nanocomposite particles are (i) spherical, (ii) decorated with a particulate silica shell and (iii) exhibit a significant range in particle size. The polystyrene/silica nanocomposite particles used in this study had a number-average diameter of 249 ± 40 nm as determined by TEM and a mean silica content of 25.5 wt. %, as judged by thermogravimetry on dried particles (silica aggregation efficiency = 86 %). The solid-state density of these nanocomposite particles was 1.23 g cm^{-3} as determined by helium pycnometry and 1.21 g cm^{-3} as calculated from the thermogravimetry data. These silica contents and particle densities correlate reasonably well with the values reported previously by Schmid *et al.* for similar polystyrene/silica nanocomposite particles prepared at 60°C.[29]

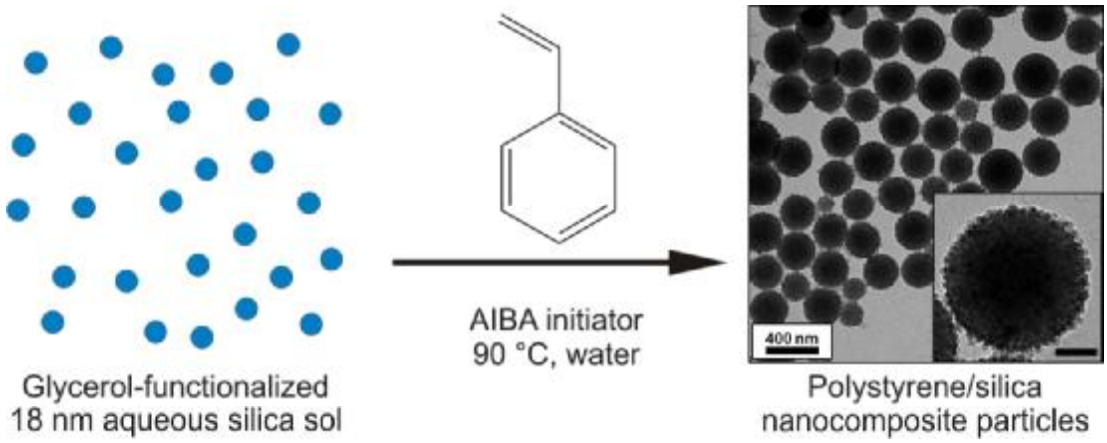

Figure 2. Schematic representation of the synthesis of polystyrene/silica nanocomposite particles by *in situ* aqueous emulsion polymerization of styrene at 90 °C in the presence of a glycerol-functionalized silica sol and a cationic azo initiator. The scale bar for the inset TEM image at higher magnification corresponds to 100 nm.

SAXS analysis and determination of the silica packing fraction. SAXS studies were conducted on a dilute aqueous dispersion of the polystyrene/silica nanocomposite particles. The scattering pattern (black squares) and the corresponding calculated fit to the data (grey line) are shown together in Figure 3. The model used to fit the data is the same as that described by Balmer *et al*.,[43] who used a two-population model based on standard analytical expressions for scattering to fit SAXS curves for a series of poly(styrene-co-*n*-butyl acrylate)/silica nanocomposite dispersions.[43] The first population defines the core-shell structure and provides both the self-correlation term for the spherical latex core and also the cross-term between this core and the silica particles within the shell. The second population involves the particulate shell alone: it describes both the self-correlation term and the cross-term for the silica particles. A range of useful parameters such as the overall core-shell nanocomposite particle diameter, the latex core diameter and associated polydispersity, the mean silica shell thickness, the mean silica diameter and associated polydispersity, the relative volume fractions of the polymer and silica components and the silica packing density within the shell could be determined.[43] Full analysis confirmed that the silica nanoparticles form a monolayer around the polymer latex core. Moreover, these SAXS data were in good agreement with results obtained using other techniques such as electron microscopy, dynamic light scattering, thermogravimetry, helium pycnometry and BET surface area analysis.[43]

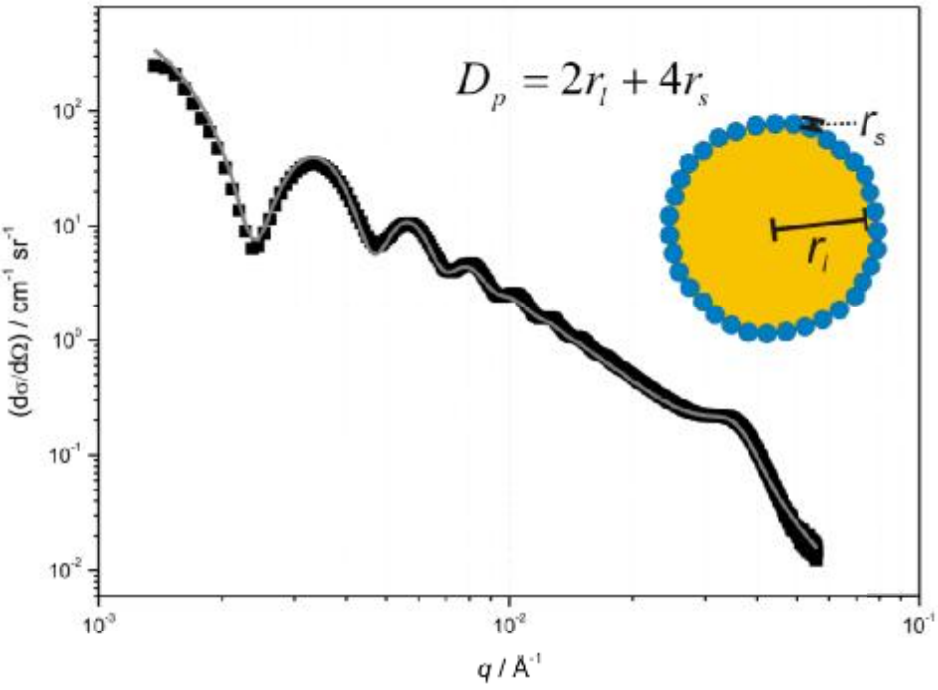

Figure 3. Desmeared SAXS scattering curve (black squares) and corresponding data fit using the two-population model (grey line) for a 1.0 wt. % aqueous dispersion of core-shell polystyrene/silica nanocomposite particles. The inset cartoon is a schematic representation of the particle morphology indicating the core radius (r_l) and shell radius (r_s) and defining the nanocomposite particle diameter, D_p, such that $D_p = 2r_l + 4r_s$

The multiple oscillations observed at low q in Figure 3 suggest that the polystyrene/silica particles used in the present study have relatively low polydispersity. Furthermore, the broad shoulder at $q \approx 0.033$ Å^{-1} corresponds to a length scale of around 19 nm, which corresponds to the centre-to-centre separation between adjacent silica particles within the nanocomposite shell. The two-population model used to fit the SAXS data obtained for these core-shell polystyrene/silica particles reports several parameters that can be compared to independent experimental data, see Table 1.

Table 1. Summary of the mean particle diameters, silica contents and silica packing density reported by small-angle x-ray scattering (SAXS), dynamic light scattering (DLS), laser diffraction, disk centrifuge photosedimentometry (DCP), transmission electron microscopy (TEM), helium pycnometry and thermogravimetry (TGA) for the core-shell polystyrene/silica nanocomposite particles used in this work.

sample	particle diameter / nm					silica content [(e)] / volume %				packing density [(f)]
	DLS [(a)]	laser diffraction	SAXS [(b)]	DCP [(c)]	TEM [(d)]	from particle density	from TGA	from SAXS [(f)]		
								structure factor	form factor	
PS/silica	317 (0.016)	287 ± 84	289 ± 34	259 ± 29	249 ± 40	16	14	15	17	0.48

(a) DLS polydispersity index is indicated in brackets. (b) The mean SAXS particle diameter was obtained from the core radius and shell thickness, the overall standard deviation was obtained from that of the core and the silica particles. (c) The density used to calculate the DCP particle diameter was 1.23 g cm^{-3}, as determined by helium pycnometry. (d) Mean TEM particle diameter was calculated by analyzing 650 particles. (e) The densities used for the polystyrene latex core and silica particles in all calculations were 1.05 and 2.16 g cm^{-3}, respectively. These values were determined by helium pycnometry. (f) As determined using the SAXS method reported by Balmer et al. in ref. 42.

As expected, the particle diameter and silica content determined by SAXS is consistent with the values determined using independent characterization techniques. In particular, the DLS intensity-average diameter is larger than the volume-average diameter reported by laser diffraction and the weight-average diameter reported by SAXS (which are in close agreement), which in turn are both larger than the number-average diameter determined by TEM. In contrast, it is noteworthy that the weight-average diameter obtained from DCP, which should correlate well with the laser diffraction and SAXS data, is *significantly* smaller than anticipated, at only 259 ± 29 nm.

The packing density (P) for the silica particles within the shell of the polystyrene/silica particles is estimated to be 0.48 from the fitted SAXS data.[43] This value is approximately the same as the packing densities previously reported for a series of analogous poly(styrene-co-*n*-butyl acrylate)/silica nanocomposite particles.[43] In this prior study, it was demonstrated that the silica packing density was more or less independent of the mean nanocomposite particle diameter. For the present work, P is therefore assumed to remain constant, regardless of the individual nanocomposite particle diameter.

Analysis of the particle density distribution. Simple geometric arguments indicate that there is a density distribution superimposed on the particle size distribution; see Figure 1. Thus the smaller nanocomposite particles within a given size distribution will necessarily have somewhat higher

densities, whilst the larger nanocomposite particles will have lower densities. Helium pycnometry is commonly used to obtain the density of dried particles by determining the dead space volume of a sample of known mass. However, this technique reports a *mean* density averaged over many millions of particles: it can provide no information regarding the possible presence of a density distribution. In contrast, Analytical ultracentrifugation (AUC) involves the sedimentation of particles at high rotational speeds in a sample cell; this leads to fractionation of the nanocomposite particles *in situ* and hence enables assessment of their density distribution.[49,50] AUC has been widely applied for the analysis of colloidal particles[49] including the study of polyelectrolyte complexes,[51] latexes,[52,53] inorganic sols[52,54-56] or hybrid particles.[50,52,57] In the present study, AUC is utilized to examine the hypothesis that core-shell polystyrene/silica particles of finite polydispersity are expected to exhibit a density distribution.

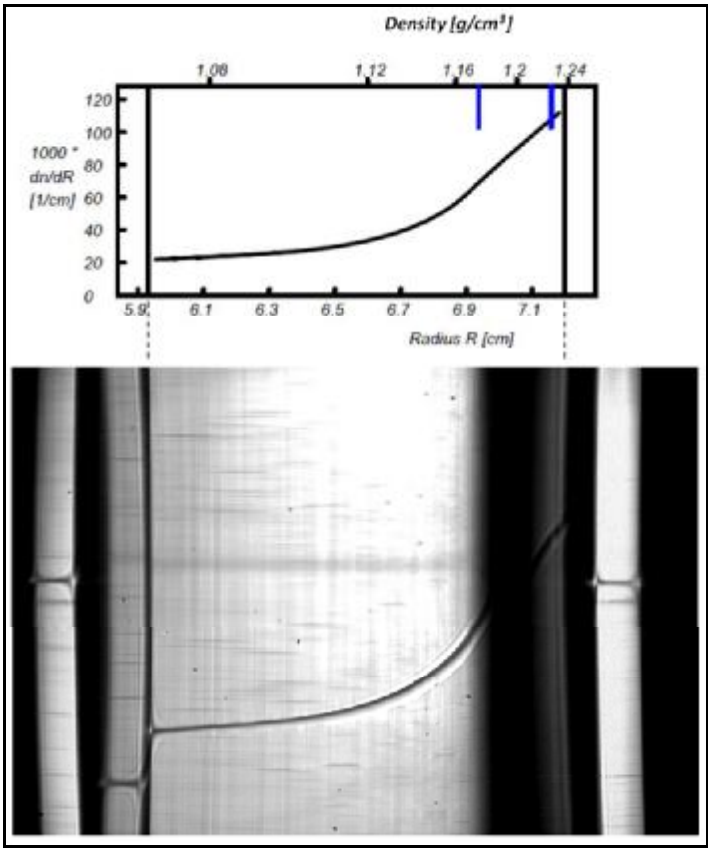

Figure 4. Schlieren image representing the density distribution of polystyrene/silica nanocomposite particles synthesized via aqueous emulsion polymerization at 90°C (density gradient, 22 h at 30 000 rpm, 25 °C, 20 wt. % Nycodenz in water, particle concentration = 0.050 wt. %).

Figure 4 shows the density distribution determined for the polystyrene/silica nanocomposite particles using AUC at 30,000 rpm for 22 h. This measurement was conducted on a 0.05 wt. % dispersion of the polystyrene/silica nanocomposite particles at room temperature using a density gradient that comprised 20 wt. % Nycodenz in water and ranged from 1.07 to 1.24 g cm^{-3}. The

Schlieren image of the polystyrene/silica nanocomposite particles (see Figure 4) shows a thick band corresponding to the fractionation of the nanocomposite particles according to their density. It was determined that the variation in particle density ranged from 1.17 to 1.23 g cm^{-3}, with a mean value of 1.20 g cm^{-3}. Thus the AUC experiment confirms that these core-shell polystyrene/silica particles do indeed exhibit a density distribution superimposed on their particle size distribution. Furthermore, this observed density range and mean value are in reasonably good agreement with the solid-state density obtained from helium pycnometry (1.23 g cm^{-3}) and also the density of 1.21 g cm^{-3} calculated from the average silica content of the nanocomposite particles indicated by TGA (assuming that the densities of polystyrene and silica are 1.05 and 2.16 g cm^{-3}, respectively).

Particle size analysis by DCP. Given that AUC confirms that these core-shell polystyrene/silica nanocomposite particles possess a density distribution, it is important to ascertain how this affects the analysis of such dispersions using DCP, for which only a single density value is required as an input parameter.

During DCP analysis, particles are separated radially through a rotating disk containing a spin fluid according to their sedimentation velocities. This velocity depends on the mass and the difference in density between the particles and the spin fluid. A light source and photodetector are placed on opposing sides of the spinning disk to detect the particles as they reach a fixed point near the disk periphery. This generates a plot of turbidity against time at a given radial distance, which can be related to the particle volume using Mie theory. Assuming a *spherical* particle morphology, this volume is then readily converted into a mean diameter provided that the effective particle density is accurately known. Since particle fractionation occurs during the measurement, DCP offers much higher resolution than either DLS or laser diffraction. Moreover, DCP is generally much more statistically robust and convenient than TEM, since typically millions of particles are analyzed within tens of minutes (rather than a few hundred within hours). However, an inherent assumption for DCP is that all particles have the same density. If this is not the case, either artificially broader or narrower particle size distributions may be reported. The latter scenario is expected for the polystyrene/silica nanocomposite particles, as the silica shell is significantly denser than the polystyrene core (see Figure 1).

Particle size distributions of the polystyrene/silica nanocomposite particles have been determined using TEM, DCP, laser diffraction and DLS (Figure 5). It is generally expected that the number-average diameter will be smaller than either the weight- or volume-average diameters, which in turn should be smaller than the intensity-average diameter. However, compared to the other three sizing techniques, the weight-average diameter of the polystyrene/silica nanocomposite particles reported by DCP is clearly both smaller and narrower than expected. The weight-average diameter reported by DCP is calculated using a single mean density value; in this case the helium pycnometry particle density of 1.23 g cm^{-3} was used. Given accurate knowledge of the density distribution, can this systematic sizing error be corrected to obtain the true weight-average particle size distribution for these polystyrene/silica nanocomposite particles?

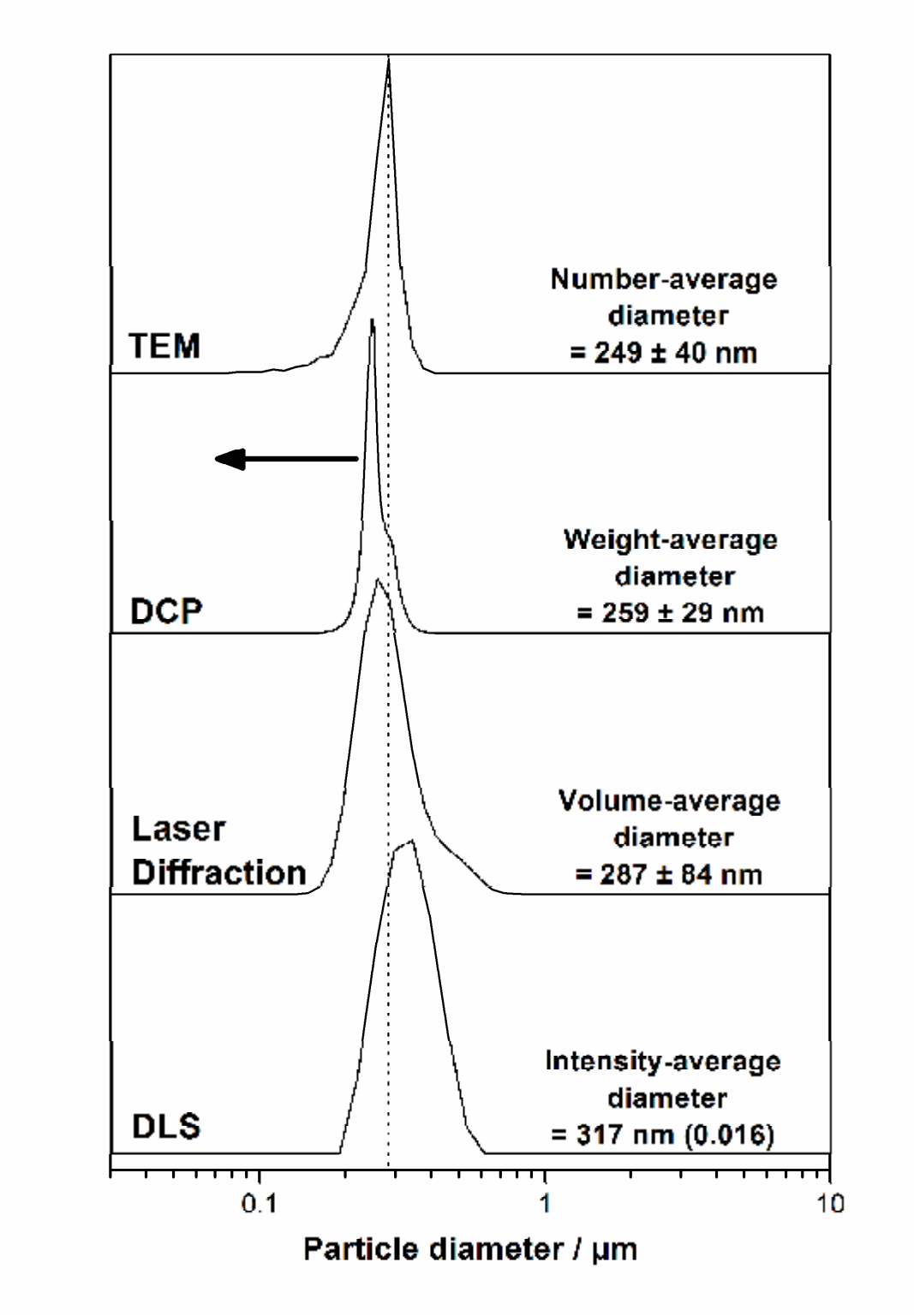

Figure 5. Various particle size distributions reported by TEM, DCP, laser diffraction and DLS for the polystyrene/silica nanocomposite particles. The TEM number-average diameter was calculated by counting 650 particles and the single density value used to determine the DCP weight-average diameter was 1.23 g cm^{-3}. Clearly there is a systematic error associated with the DCP analysis, since this size distribution is shifted to the left of the TEM size distribution. Note that the former distribution is also significantly narrower than those reported by the other three techniques.

Method for correcting the DCP particle size distribution. If the polystyrene/silica nanocomposite particles do not all have the same density (see Figure 1), the apparent DCP diameter will in general differ from the true weight-average particle diameter. The following treatment shows how, for particles with a core-shell morphology, the size distribution can be corrected for the known variation in density with particle diameter. The treatment is purely analytical, in that the correction is derived by solving a polynomial equation whose coefficients depend only on the particle morphology and the physical properties and dimensions of the core and shell components.

The CPS disk centrifuge measures optical absorption at a fixed standard wavelength as a function of time of detection. If the particle density is assumed to be independent of particle size, Stokes theory can be used to deduce the particle diameter from the detection time. This derived information is combined with Mie theory to predict the light absorption as a function of diameter, and hence to derive the weight-average particle diameter.

For particles of uniform density ρ moving according to Stokes' Law through a spin fluid of density ρ_f, the relationship between the time of detection (t) and the apparent diameter (D_t) of the particles detected at that time is given by

$$\Delta_0 D_t^2 = C/t \tag{1}$$

where Δ_0 is the density difference ($\rho - \rho_f$), and C is a constant determined by the viscosity of the fluid, the spin speed and the cell geometry. In the usual mode of operation, this constant is determined by comparison with a reference sample of known diameter, a suitable value for the particle density ρ is selected, and the instrument software then computes D_t as a function of time.

If the particles do not all have the same density, an average particle density can be used in (1), but then the predicted diameter D_t will in general differ from the true particle diameter, D_p. For particles with a core-shell morphology, such as the nanocomposite particles studied here, the true diameter for particles detected at time t is given by

$$D_p = 2r_l + 4r_s \tag{2}$$

where r_l and r_s are, respectively, the radii of the (latex) core and the (silica) spheres that compose the outer shell (see Figure 3).

The true particle density is a function of these two radii and also the intrinsic densities of the polystyrene and silica. The density of a core-shell particle composed of N silica spheres surrounding a central polystyrene latex core is given by

$$\rho_p = \frac{N\rho_s r_s^3 + \rho_l r_l^3}{N r_s^3 + r_l^3} \tag{3}$$

Thus the relationship between the detection time and true diameter, D_p, is then

$$\Delta_p D_p^2 = (\rho_p - \rho_f)(2r_l + 4r_s)^2 = \frac{C}{t} = \Delta_0 D_t^2 \tag{4}$$

The silica particles are much smaller than the latex core (typically $r_l / r_s > 20$), hence

$$r_l / r_s >> 1, \tag{5}$$

If we further assume a fixed packing density *P* (which is reasonable in view of the SAXS data reported by Balmer *et al*.[43]), the number of silica particles per polystyrene latex core can be approximated as[58]

$$N = 4P(r_l + r_s)^2 / r_s^2 = 4P(1+r)^2 \tag{6}$$

where *r* is the dimensionless variable $r = (r_l / r_s)$. Therefore, substitution of (6) and (3) into (4) provides the core radius r_l as a multiple of the silica particle radius, given the apparent diameter D_t, and hence the true particle diameter D_p can be calculated. With these substitutions, the expanded form of (4) yields a quintic equation in the dimensionless variable, *r*, of the form:

$$g(r) = ar^5 + br^4 + cr^3 + dr^2 + er + f = 0 \tag{7}$$

where the six coefficients are expressed as follows:

$a = 1$

$$b = 4 + 4P\Delta_s / \Delta_l$$

$$c = 4 + 24P(\Delta_s / \Delta_l) - \tfrac{1}{4}(\Delta_0 / \Delta_l)(D_t / r_s)^2$$

$$d = 52P(\Delta_s / \Delta_l) - P(\Delta_0 / \Delta_l)(D_t / r_s)^2$$

$$e = 48P(\Delta_s / \Delta_l) - 2P(\Delta_0 / \Delta_l)(D_t / r_s)^2$$

$$f = 16P(\Delta_s / \Delta_l) - P(\Delta_0 / \Delta_l)(D_t / r_s)^2 \tag{8}$$

As a quintic equation with real coefficients, (7) must have either one, three or five real roots, i.e., values of *r** for which g(*r**) = 0. Descartes' Rule of Signs[59] places a limitation on the number of positive (and therefore physically acceptable) real roots: if the number of sign changes between consecutive members of the sequence of coefficients [*c*, *d*, *e*, *f*] is *p*, there are either *p* or *p*–2 or *p*–4 positive real roots of (7). The various expressions in (8) show that $a > 0$, $b > 0$ and that the other coefficients have signs that are determined by competition between terms. For sufficiently large D_t, all the remaining coefficients are negative: $c < 0$, $d < 0$, $e < 0$, $f < 0$. Thus, at least for the large-diameter, short-time regime, there is a *unique physically acceptable* solution for r and hence D_p.

Typical values for the polystyrene/silica nanocomposite particles are $(\Delta_s / \Delta_0) \approx 5$, $(\Delta_p / \Delta_0) \approx 1/10$, and $r_l > 10\, r_s$. Negative signs for coefficients *c*, *d*, *e*, *f* imply respective approximate bounds of $D_t > 22 r_s$, $D_t > 16 r_s$, $D_t > 11 r_s$, $D_t > 9 r_s$. As $r_l > 10 r_s$ gives $D_p > 24 r_s$, and since we can expect $D_t \approx D_p$, the bounds are easily met in the region of significant optical absorption. Solution of (7) to find the unique physical solution for a given choice of the silica packing density, *P*, is therefore straightforward. For example, it can be achieved by applying the robust Newton-Raphson method,[60] where an initial guess is iteratively improved according to the formula:

$$r^{(n+1)} = r^{(n)} - g(r^{(n)}) / g'(r^{(n)}) \quad (9)$$

where $g'(r) = \mathrm{d}g / dr$ and an appropriate starting guess could be $r^{(0)} = \frac{1}{2} D_t - 2$.

Once a value of D_p has been obtained from each D_t, the curve for the scattering cross-section as a function of diameter, $Q_{net}(D)$, can be used to convert the measured absorption vs. time profile into a corrected particle size distribution. The scattering cross section, $Q_{net}(D)$, is determined by the optical properties of the particles. In the present case, the function used by the CPS instrument software for polystyrene latex particles was taken to apply also to the composite particles, and was found to be well represented by a sextic polynomial fitting function. Another approach would be to use the function for silica provided by the instrument software. In fact, this choice makes no discernible difference to the calculated size distribution, at least in this particular case.

Recalculation of the DCP particle size distribution. In order to recalculate the true weight-average particle size distribution for the polystyrene/silica particles by DCP, a computer program was written to perform the calculation based on the method described above (see Supporting Information for further details of this program). Thus for a given set of absorption versus time values obtained from DCP and for a set of fixed input parameters, the true particle size distribution can readily be recalculated. The input parameters used for the polystyrene/silica nanocomposite particles were the densities of silica, polystyrene, aqueous sucrose spin fluid and the mean nanocomposite density used in the original DCP analysis (2.16 g cm^{-3}, 1.05 g cm^{-3}, 1.03 g cm^{-3} and 1.23 g cm^{-3} respectively); the packing density of the silica particles (0.48); and the mean radius of the silica particles (8.8 nm). It should be noted that an accurate silica packing density *P* is crucial for calculating the density of individual nanocomposite particles. As discussed above, this key structural parameter was determined from SAXS analysis.

The values generated by the computer program were readily manipulated using an *Excel* spreadsheet into a format which could be read by the DCP operating software (CPS control software, version 9.5c) and the corrected particle size distribution for the polystyrene/silica nanocomposite particles was calculated; see Figure 6(c). The original particle size distribution obtained using the single helium pycnometry density value (1.23 g cm^{-3}) is also plotted (see Figure 6a), along with a crude correction made using the mid-range density of 1.20 g cm^{-3} obtained from AUC (see Figure 6b). For single density values (a, b), the particle size distribution is significantly narrower than that shown in (c). This artificial narrowing is a direct result of the intrinsic density distribution possessed by such core-shell nanocomposite particles. Moreover, this recalculated DCP particle size distribution is now much more consistent in terms of both its weight-average diameter and width with the size distributions obtained using density-independent techniques such as TEM, laser diffraction and DLS. Inspecting the three traces, the crude 'mid-point density from AUC' correction is sufficient to obtain a more accurate weight-average diameter, but this approach cannot compensate for the artificial narrowing of the DCP size distribution that is observed in the absence of an appropriate density distribution correction. Notably, the standard deviation for the final density distribution-corrected DCP particle size distribution is approximately twice that of the two size distributions computed using single density values.

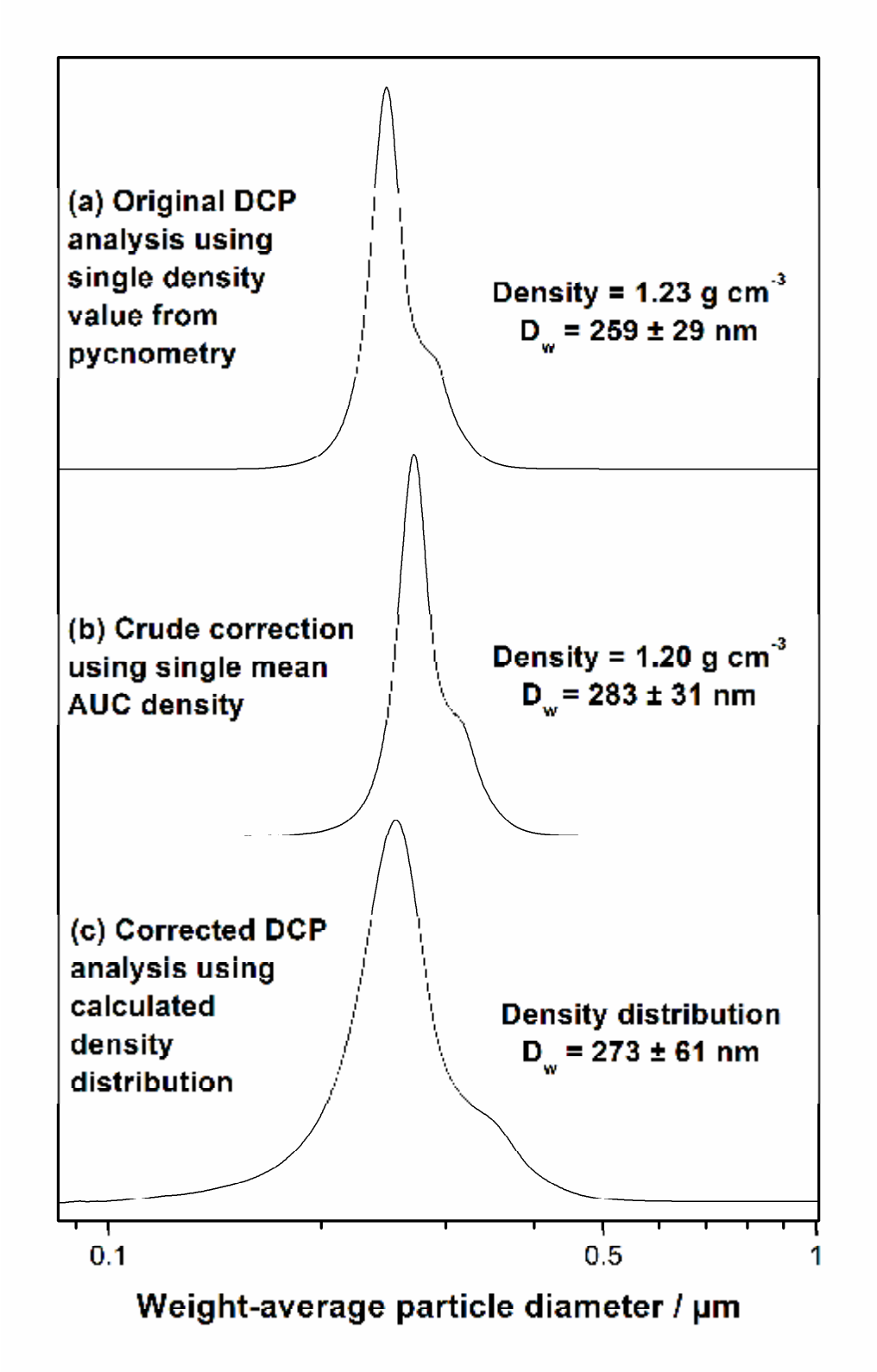

Figure 6. Particle size distributions of polystyrene/silica nanocomposite particles calculated from a single DCP analysis using: (a) a mean helium pycnometry density of 1.23 g cm^{-3}; (b) a single density value of 1.20 g cm^{-3} taken from the mid-point of the AUC density distribution; (c) a density distribution calculated assuming a silica packing fraction of 0.48, a silica density of 2.16 g cm^{-3} and a polystyrene density of 1.05 g cm^{-3}.

Clearly, the relationship between the overall nanocomposite particle diameter (D_p) and particle density (ρ_p) is important in determining the extent to which the corrected DCP size distribution differs from that calculated using a single density. To illustrate this point more clearly, the calculated density profile for the polystyrene/silica particles analyzed in this study is shown in Figure 7. As expected, smaller nanocomposite particles have higher calculated densities than larger particles. The precise relationship is given by equation (3), which for convenience is reproduced within Figure 7. It is noteworthy that the most pronounced variation in particle density occurs for smaller diameters: very little change in density with size is observed for relatively large particles (> 1 μm diameter), as their silica volume fraction is almost negligible.

In the current study, the size regime for the polystyrene/silica particles (see Figure 7) is such that the variation in density with particle diameter is sufficient to produce a significant artifact in the DCP size distribution. More specifically, the particle density range of 1.17 to 1.23 g cm^{-3} determined by AUC corresponds to calculated maximum and minimum particle diameters of 346 and 240 nm, respectively.

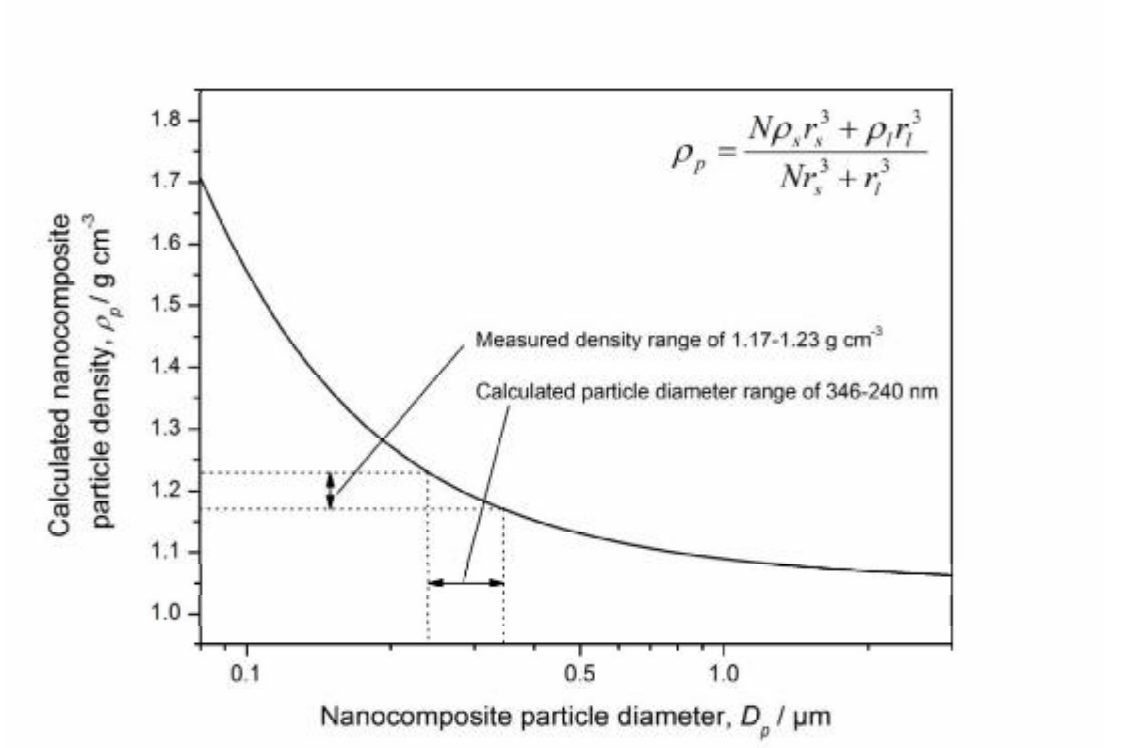

Figure 7. Relationship between particle density (ρ_p) and particle diameter (D_p) for the polystyrene/silica nanocomposite particles analyzed in this work. The particle density was calculated assuming a fixed silica particle radius of 8.8 nm, a silica packing fraction of 0.48, a silica density of 2.16 g cm^{-3} and a polystyrene density of 1.05 g cm^{-3}. Analytical ultracentrifugation studies indicate a particle density range of 1.17-1.23 g cm^{-3}, which corresponds to a particle size range of 240-346 nm.

General remarks. As noted above, the main criterion for the observation of this artifact in DCP measurements is that composite particles should exhibit a significant variation in density with particle size. Moreover, this artifact will be a general problem for core-shell particles where the two

components have comparable masses, but there is an appreciable difference between the core and shell densities. This is most likely to occur for various types of core-shell organic-inorganic nanocomposite particles where the inorganic shell is relatively dense (e.g. titania, magnetite, zirconia, zinc oxide, gold).

Other examples of core-shell particles likely to be affected include latexes that combine low-density cores (e.g., polystyrene) with high-density shells (e.g., poly(4-bromostyrene), which has a relatively high density of 1.62 g cm^{-3}). In this latter case it is likely that the shell layer will be more or less uniform (rather than particulate) in nature. This will alter (actually simplify) the details of the required mathematical correction, but the fundamental problem for DCP analysis created by the manifestation of a particle density distribution will remain. We intend to analyze this 'uniform shell' situation in more detail and report our findings elsewhere in due course. Another important parameter that influences the magnitude of the sizing error is the polydispersity.

In principle, highly monodisperse core-shell particles (possessing uniform cores and shells) should suffer much less from this artifact, regardless of the difference between the core and shell densities. Furthermore, the artifact is also likely to be insignificant when the density does not vary over the size range of interest. In Figure 7, this occurs for diameters above approximately 1 µm and corresponds to the limit where the silica volume fraction of the nanocomposite particles is becoming negligible. Similarly, if there is relatively little density difference between the core and shell components the raw DCP particle size distribution should not require correction. In particular, most commercial core-shell copolymer latexes used in industrial paint formulations are unlikely to possess a sufficiently large density difference to introduce significant DCP sizing errors.

In summary, due care should be exercised when analyzing colloidal particles by DCP in order to ensure that meaningful particle size distributions are reported. In many cases, the choice of a single density value for the particles will lead to sufficiently accurate and reliable data. However, for core-shell particles the possible variation in particle density with diameter should be considered and, where this is deemed significant, the relevant mathematical correction should be applied. Given that the accurate particle size analysis of nanoparticles is likely to be of regulatory importance in the future, we believe that the rigorous elimination of this DCP artifact when sizing core-shell particles is likely to have wider implications.[61,62]

Conclusions

Well-defined core-shell nanocomposite particles of finite polydispersity that possess a significant difference in density between the core and shell components must inevitably have a density distribution superimposed on their particle size distribution. This density distribution can be determined directly using analytical ultracentrifugation. In the specific case of polystyrene/silica nanocomposite particles, this leads to an artificial narrowing of the particle size distribution determined by disk centrifuge photosedimentometry, which is normally considered to be a reliable and convenient high resolution sizing technique. Using a silica packing density determined by SAXS studies, the silica diameter and the known densities of the polystyrene and silica components, this experimental artifact can be readily corrected using a simple computer program. The recomputed particle size distribution is shown to be consistent with data determined by other sizing techniques

provided that due allowance is made for the individual bias of each method. This artifact will always occur for core-shell particles where there is an appreciable difference between the core and shell densities and a shell of constant thickness surrounds a core of variable dimensions. Moreover, this problem is likely to be exacerbated for core-shell particles with a relatively high size polydispersity.

Acknowledgments

The University of Sheffield is thanked for funding a PhD studentship for LAF. The authors are grateful to ESRF for providing the SAXS beam-time and also thank the personnel of ID02 station for their assistance with the SAXS experiments. Dr. J. A. Balmer and Dr. C. Fairgrieve are also acknowledged for their help with the SAXS studies. Dr. P. Greenwood of Eka Chemicals (Bohus, Sweden) is thanked for donating the aqueous silica sol. Dr. S. Lascelles is acknowledged for conducting laser diffraction measurements. Both Dr. H. Vegad and Dr I. Laidlaw of Analytik Ltd. UK are thanked for helpful technical discussions regarding the underlying theory and basic principles of the CPS disk centrifuge instrument.

Supporting Information Available. Fortran77 source code for recalculating particle size distribution of polystyrene/silica nanocomposite particles. This material is available free of charge via the Internet at http://pubs.acs.org.

References

(1) Zerrouki, D.; Rotenberg, B.; Abramson, S.; Baudry, J.; Goubault, C.; Leal-Calderon, F.; Pine, D. J.; Bibette, M. *Langmuir* **2006**, *22*, 57.

(2) Colard, C. A. L.; Teixeira, R. F. A.; Bon, S. A. F. *Langmuir* **2010**, *26*, 7915.

(3) Subramanian, R.; Zhu, S.; Pelton, R. H. *Colloid Polymer Science* **1999**, *277*, 939.

(4) Ramirez-Garcia, S.; Chen, L.; Morris, M. A.; Dawson, K. A. *Nanoscale* **2011**, *3*, 4617.

(5) Vamvakaki, M.; Billingham, N. C.; Armes, S. P.; Watts, J. F.; Greaves, S. J. *J. Mater. Chem.* **2001**, *11*, 2437.

(6) Nadler, M.; Mahrholz, T.; Riedel, U.; Schilde, C.; Kwade, A. *Carbon* **2008**, *46*, 1384.

(7) Brugger, K. *Powder Technol.* **1976**, *13*, 215.

(8) Thomas, J. C.; Middelberg, A. P. J.; Hamel, J. F.; Snoswell, M. A. *Biotechnol. Prog.* **1991**, *7*, 377.

(9) Middelberg, A. P. J.; Bogle, I. D. L.; Snoswell, M. A. *Biotechnol. Prog.* **1990**, *6*, 255.

(10) Bondoc, L. L.; Fitzpatrick, S. *J. Ind. Microbiol. Biotechnol.* **1998**, *20*, 317.

(11) Verdurmen, E. M.; Albers, J. G.; German, A. L. *Colloid Polymer Science* **1994**, *272*, 57.

(12) Dupin, D.; Fujii, S.; Armes, S. P.; Reeve, P.; Baxter, S. M. *Langmuir* **2006**, *22*, 3381.

(13) Dupin, D.; Howse, J. R.; Armes, S. P.; Randall, D. P. *J. Mater. Chem.* **2008**, *18*, 545.

(14) Walczyk, D.; Bombelli, F. B.; Monopoli, M. P.; Lynch, I.; Dawson, K. A. *J. Am. Chem. Soc.* **2010**, *132*, 5761.

(15) Bucsi, A.; Forcada, J.; Gibanel, S.; Heroguez, V.; Fontanille, M.; Gnanou, Y. *Macromolecules* **1998**, *31*, 2087.

(16) Elizalde, O.; Leal, G. P.; Leiza, J. R. *Part. Part. Syst. Charact.* **2000**, *17*, 236.

(17) Kohler, J. M.; Wagner, J.; Albert, J. *J. Mater. Chem.* **2005**, *15*, 1924.

(18) Krpetic, Z.; Porta, F.; Caneva, E.; Dal Santo, V.; Scari, G. *Langmuir* **2010**, *26*, 14799.

(19) Gill, M.; Armes, S. P.; Fairhurst, D.; Emmett, S. N.; Idzorek, G.; Pigott, T. *Langmuir* **1992**, *8*, 2178.

(20) Maeda, S.; Armes, S. P. *J. Mater. Chem.* **1994**, *4*, 935.

(21) Maeda, S.; Corradi, R.; Armes, S. P. *Macromolecules* **1995**, *28*, 2905.
(22) Han, M. G.; Armes, S. P. *Langmuir* **2003**, *19*, 4523.
(23) Han, M. G.; Armes, S. P. *J. Colloid Interface Sci.* **2003**, *262*, 418.
(24) Percy, M. J.; Barthet, C.; Lobb, J. C.; Khan, M. A.; Lascelles, S. F.; Vamvakaki, M.; Armes, S. P. *Langmuir* **2000**, *16*, 6913.
(25) Percy, M. J.; Amalvy, J. I.; Randall, D. P.; Armes, S. P.; Greaves, S. J.; Watts, J. F. *Langmuir* **2004**, *20*, 2184.
(26) Schmid, A.; Fujii, S.; Armes, S. P. *Langmuir* **2006**, *22*, 4923.
(27) Schmid, A.; Fujii, S.; Armes, S. P.; Leite, C. A. P.; Galembeck, F.; Minami, H.; Saito, N.; Okubo, M. *Chem. Mater.* **2007**, *19*, 2435.
(28) Schmid, A.; Tonnar, J.; Armes, S. P. *Adv. Mater.* **2008**, *20*, 3331.
(29) Schmid, A.; Armes, S. P.; Leite, C. A. P.; Galembeck, F. *Langmuir* **2009**, *25*, 2486.
(30) Fielding, L. A.; Tonnar, J.; Armes, S. P. *Langmuir* **2011**, *27*, 11129.
(31) Balmer, J. A.; Le Cunff, E. C.; Armes, S. P. *Langmuir* **2010**, *26*, 13662.
(32) Barthet, C.; Armes, S. P.; Lascelles, S. F.; Luk, S. Y.; Stanley, H. M. E. *Langmuir* **1998**, *14*, 2032.
(33) Schmid, A.; Sutton, L. R.; Armes, S. P.; Bain, P. S.; Manfre, G. *Soft Matter* **2009**, *5*, 407.
(34) Khan, M. A.; Armes, S. P. *Langmuir* **1999**, *15*, 3469.
(35) Monopoli, M. P.; Walczyk, D.; Campbell, A.; Elia, G.; Lynch, I.; Baldelli Bombelli, F.; Dawson, K. A. *J. Am. Chem. Soc.* **2011**, *133*, 2525.
(36) Dupin, D.; Schmid, A.; Balmer, J. A.; Armes, S. P. *Langmuir* **2007**, *23*, 11812.
(37) Fujii, S.; Armes, S. P.; Binks, B. P.; Murakami, R. *Langmuir* **2006**, *22*, 6818.
(38) Burchell, M. J.; Willis, M. J.; Armes, S. P.; Khan, M. A.; Percy, M. J.; Perruchot, C. *Planet. Space Sci.* **2002**, *50*, 1025.
(39) Fujii, S.; Armes, S. P.; Jeans, R.; Devonshire, R.; Warren, S.; McArthur, S. L.; Burchell, M. J.; Postberg, F.; Srama, R. *Chem. Mater.* **2006**, *18*, 2758.
(40) Xue, Z.; Wiese, H. **2006**, United States Patent US7094830B2.
(41) Amalvy, J. I.; Percy, M. J.; Armes, S. P.; Leite, C. A. P.; Galembeck, F. *Langmuir* **2005**, *21*, 1175.
(42) Percy, M. J.; Amalvy, J. I.; Barthet, C.; Armes, S. P.; Greaves, S. J.; Watts, J. F.; Wiese, H. *J. Mater. Chem.* **2002**, *12*, 697.
(43) Balmer, J. A.; Mykhaylyk, O. O.; Schmid, A.; Armes, S. P.; Fairclough, J. P. A.; Ryan, A. J. *Langmuir* **2011**, *27*, 8075.
(44) Balmer, J. A.; Mykhaylyk, O. O.; Armes, S. P.; Fairclough, J. P. A.; Ryan, A. J.; Gummel, J.; Murray, M. W.; Murray, K. A.; Wiliams, N. S. J. *J. Am. Chem. Soc.* **2011**, *133*, 826.
(45) Balmer, J. A.; Mykhaylyk, O. O.; Fairclough, J. P. A.; Ryan, A. J.; Armes, S. P.; Murray, M. W.; Murray, K. A.; Williams, N. S. J. *J. Am. Chem. Soc.* **2010**, *132*, 2166.
(46) Borger, L.; Lechner, M. D.; Stadler, M. In *Analytical Ultracentrifugation Vii*; Lechner, M. D., Borger, L., Eds. 2004; Vol. 127, p 19.
(47) Machtle, W.; Lechner, M. D. In *Analytical Ultracentrifugation Vi*; Borchard, E., Straatmann, A., Eds. 2002; Vol. 119, p 1.
(48) Sztucki, M.; Narayanan, T. *J. Appl. Crystallogr.* **2007**, *40*, S459.
(49) Planken, K. L.; Colfen, H. *Nanoscale* **2010**, *2*, 1849.
(50) Mittal, V. *Colloid Polymer Science* **2010**, *288*, 621.
(51) Karibyants, N.; Dautzenberg, H.; Colfen, H. *Macromolecules* **1997**, *30*, 7803.
(52) Mittal, V.; Lechner, M. D. *J. Colloid Interface Sci.* **2010**, *346*, 378.
(53) Mittal, V. *Colloid Polymer Science* **2010**, *288*, 25.
(54) Colfen, H.; Pauck, T. *Colloid Polymer Science* **1997**, *275*, 175.
(55) Colfen, H.; Schnablegger, H.; Fischer, A.; Jentoft, F. C.; Weinberg, G.; Schlogl, R. *Langmuir* **2002**, *18*, 3500.

(56) Mittal, V.; Volkel, A.; Colfen, H. *Macromol. Biosci.* **2010**, *10*, 754.

(57) Jamison, J. A.; Krueger, K. M.; Yavuz, C. T.; Mayo, J. T.; LeCrone, D.; Redden, J. J.; Colvin, V. L. *ACS Nano* **2008**, *2*, 311.

(58) Balmer, J. A.; Armes, S. P.; Fowler, P. W.; Tarnai, T.; Gáspár, Z.; Murray, K. A.; Williams, N. S. J. *Langmuir* **2009**, *25*, 5339.

(59) Weisstein, E. W. *CRC Concise Encyclopedia of Mathematics*; 2nd ed.; CRC Press: Boca Raton, FL, 2002.

(60) Press, W. H.; Flannery, B. P.; Teukolsky, S. A.; Vetterling, W. T. *Numerical Recipes in FORTRAN, The Art of Scientific Computing*; 2nd ed.; Cambridge University Press: Cambridge, 1992.

(61) *Nanoscience and Nanotechnologies: Opportunities and Uncertainties, The Royal Society* **2004**.

(62) *SCENIHR (Scientific Committee on Emerging and Newly Identified Health Risks), Opinion*

on the scientific basis for the definition of the term "nanomaterial", 8 December 2010.

TOC Graphic for Langmuir manuscript: